



Fabrication of spinel CoMn_2O_4 hollow spheres for highly selective aerobic oxidation of 5-hydroxymethylfurfural to 2,5-diformylfuran

Lei Ding, Wenyu Yang, Lifang Chen*, Hongye Cheng, Zhiwen Qi

State Key Laboratory of Chemical Engineering, School of Chemical Engineering, East China University of Science and Technology, Shanghai 200237, China

ARTICLE INFO

Keywords:

5-hydroxymethylfurfural
2,5-diformylfuran
Selective oxidation
Spinel CoMn_2O_4
Hollow spheres

ABSTRACT

Spinel CoMn_2O_4 hollow spheres were prepared by a solvothermal method, where uniform cobalt-manganese glycerate spheres as the precursor were self-assembled and converted into hollow spheres by calcination. The as-prepared catalysts were characterized by field emission scanning electron microscopy (FESEM), X-ray powder diffraction (XRD), X-ray photoelectron spectroscopy (XPS), nitrogen adsorption and desorption isotherms, thermogravimetric analysis, and H_2 temperature programmed reduction (H_2 -TPR). The results show that body-centered tetragonal and face-centered cubic spinel structures of CoMn_2O_4 hollow spheres can be tuned by different Co/Mn molar ratios. Moreover, the spinel CoMn_2O_4 hollow spheres exhibit high catalytic activity for the selective oxidation of 5-hydroxymethylfurfural (HMF) into 2,5-diformylfuran (DFF). Importantly, the spinel CoMn_2O_4 hollow spheres with Co/Mn molar ratio of 2/3 shows the highest catalytic performance with a 41.6% HMF conversion and a 100% selectivity to DFF. On one hand, the spinel CoMn_2O_4 hollow spheres with large surface area have sufficient exposed active sites for the oxidation of HMF and oxidized product DFF can fast leave the catalyst surface leading to high selectivity, avoiding further oxidation. On the other hand, the synergistic effect between Co and Mn species in the binary oxides by the formation of heteronuclear cluster complexes CoMn_2O_4 , which affects and promotes the electron-transfer process, results in significant improvement in catalyst performance. Additionally, the effects of different Co/Mn molar ratios, catalyst amounts, reaction time and temperatures of the catalyst for HMF oxidation were also investigated. Furthermore, the spinel CoMn_2O_4 hollow spheres can be used for six consecutive runs without significant loss of its catalytic activity.

1. Introduction

The main sources of functional carbon skeletons including fuels and chemicals highly rely on fossil resources such as coal, petroleum, and natural gas [1]. In view of the fast depletion of fossil resources and increasing environmental concerns, the development of efficient and greener processes for the production of chemicals and fuels from renewable biomass has attracted growing interests over the last decade. Biomass platform compounds can be effectively converted into high value chemicals and fuels, which is an ideal alternative to fossil resources. As the only sustainable source of carbon or organic compounds, biomass has been regarded as equivalent to petroleum for the production of fuels and chemicals [2–4].

As one of the most valuable platform chemicals between biomass and specialty chemicals, 5-hydroxymethylfurfural (HMF) can be obtained from lignocellulosic biomass conversion in the dehydration of fructose and glucose using acid catalysts (see Fig. 1) [5]. It has multiple functional groups containing hydroxyl, carbonyl, formyl, and furan

ring, which open a promising avenue for chemical reactions. Thus, HMF with function groups can be oxidized to produce high value-added chemicals of industrial importance, such as 2,5-diformylfuran (DFF), 5-formylfuroic acid (FFCA), 5-hydroxymethylfuroic acid (HMFCA), 2,5-furandicarboxylic acid (FDCA), and other useful compounds e.g. levulinic acid (LA), formic acid, and fumaric acid (FA) through ring opening [6]. Typically, DFF is one of the selective oxidative products of HMF with important commercial value, and can be used for the synthesis of various poly-schiff bases, pharmaceuticals, organic conductor, and cross-linking agents of poly (vinyl alcohol) for battery separations [7]. In consideration of the complexity of the HMF reaction pathway shown in Fig. 1, the development of high selectivity and efficient catalytic procedure for the synthesis of DFF from HMF is highly desirable.

Compared with homogeneous catalysts, heterogeneous metal oxides, supported noble metal and metal catalysts with many advantages of readily separation and reusability, are successfully used in various organic transformations [8]. Noble metal catalysts with moderate reaction conditions and high catalytic activity become a research

* Corresponding author.

E-mail address: lchen@ecust.edu.cn (L. Chen).

<https://doi.org/10.1016/j.cattod.2018.04.069>

Received 28 February 2018; Received in revised form 24 April 2018; Accepted 30 April 2018
0920-5861/ © 2018 Elsevier B.V. All rights reserved.

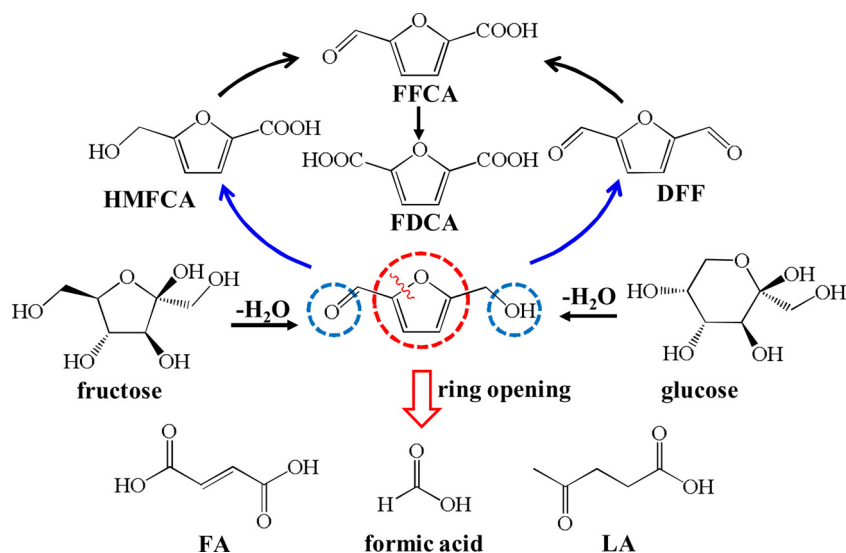


Fig. 1. Reaction pathway for aqueous HMF oxidation.

hotspot. Au, Ag, Ru, Pt, and alloy catalysts have much effect on the selective oxidation of HMF into DFF [9–13]. For instance, Au nanoparticles supported on MnO_2 afforded an 82% conversion of HMF and a 99% selectivity of DFF at 120 °C within 8 h reaction time under O_2 atmosphere [10]. Yadav et al. reported Ag-OMS-2 (OMS: octahedral molecular sieve) as a catalyst for selective oxidation of HMF with a high DFF yield of 99% at 165 °C within 4 h reaction time under 15 atm of air [11]. Ruthenium nanoparticles supported on N-containing mesoporous polymer was synthesized and excellent conversion of HMF (99.6%) and 85% DFF yield were obtained under optimized reaction conditions [12]. Our group also prepared bimetallic Au-Pd alloys supported on zinc hydroxycarbonate with excellent catalytic activity towards HMF oxidation in the presence of weak base NaHCO_3 solution at benign conditions. Although these noble metal-based catalysts generally give relatively high yields of DFF, drawbacks for this kind of catalysts are conspicuous, such as high cost and stability problems. To promote the conversion of HMF into DFF to a practical application level, it is necessary to develop efficient non-noble metal catalysts with the merits of low price, low toxicity and high stability.

Therefore, transition metal based heterogeneous catalysts for the synthesis of DFF from HMF are widely-studied [14–19]. Yang et al. synthesized a series of 3D flower-like micro/nano Ce-Mo composite oxide catalysts, which could reach a 94% DFF yield in 10 h [14]. Heterogeneous mesoporous manganese/cobalt oxide catalysts were applied to the selective oxidation of HMF into DFF with 80% conversion and 96% selectivity using air as the sole oxidant [15]. Meanwhile, the catalytic performance of a series of zeolite-supported vanadia catalysts was examined for the aerobic oxidation of HMF to DFF in organic solvents such as N,N-dimethylformamide (DMF), methyl isobutyl ketone, toluene, trifluorotoluene, and dimethyl sulfoxide (DMSO). Under optimized conditions, a high selectivity towards DFF of 99% and an 84% HMF conversion were obtained [16]. In addition, manganese-copper layered double hydroxides prepared by co-precipitation method were investigated for the selective oxidation of HMF into DFF. It has been found that a composition corresponding to $\text{Mn}_{0.70}\text{Cu}_{0.05}\text{Al}_{0.25}$ leads to the highest HMF conversion (90%) and DFF selectivity (87%) [17]. Another interesting finding is that the morphology of transition metal catalysts has a certain effect on catalytic activity [20], such as 3D flower-like micro/nano and mesoporous mentioned above. It is of great significance to improve the catalytic performance through controllable synthesis of catalysts with special shapes.

As an important family of functional materials, hollow structures are widely used in photocatalytic reactions [21,22], microwave

absorptions [23,24], ion battery electrodes [25,26], and oxygen reductions or evolution reactions [27,28] due to their excellent performance with large surface area, reduced mass and charge transport [29]. In this work, a series of spinel CoMn_2O_4 hollow spheres were synthesized using a facile solvothermal approach combined with subsequent calcination and examined for the selective oxidation of HMF into DFF. In addition, the as-synthesized spinel CoMn_2O_4 hollow spheres catalysts were characterized and the influencing factors of the selective aerobic oxidation were explored.

2. Experimental

2.1. Preparation of spinel CoMn_2O_4 hollow spheres

All chemicals used in the experiments were of analytical grade, and used without further purification. Spinel CoMn_2O_4 hollow spheres were prepared by a hydrothermal process as described in the followings. In a typical procedure, 0.80 mmol of $\text{Co}(\text{NO}_3)_2 \cdot 6\text{H}_2\text{O}$ (0.232 g) and 1.20 mmol of $\text{Mn}(\text{NO}_3)_2 \cdot 4\text{H}_2\text{O}$ (0.301 g) were dissolved in 50.5 mL of isopropanol (IPA) to form a clear solution. Then 7.5 mL of glycerol (Gly) and 2 mL of deionized (DI) water were added into the solution. After stirring for another 10 min, the solution was put into a 100 mL Teflon-lined stainless steel autoclave and kept in a muffle furnace at 190 °C for 12 h. Cooling down to room temperature naturally, the precipitate was separated by centrifugation, washed several times with ethanol and dried in an oven at 70 °C for 10 h. Finally, the precipitate was calcined at 350 °C for 3 h to obtain product named CoMn_2O_4 -2:3. A series of spinel hollow spheres were prepared by changing Co-Mn precursor molar ratios named CoMn_2O_4 -1:2, CoMn_2O_4 -1:1, CoMn_2O_4 -2:1. Besides, Mn_3O_4 , Co_3O_4 , and mechanical mixed Mn_3O_4 - Co_3O_4 were also prepared for comparison using similar method above.

2.2. Catalyst characterization

X-ray diffraction (XRD) patterns were recorded on a D8 Advance diffractometer equipped with a $\text{CuK}\alpha$ radiation source ($\lambda = 1.54056 \text{ \AA}$), operating at 40 kV and 40 mA. A continuous mode was used for collecting data in the 2θ range from 10° to 80° at a scanning speed of $10^\circ \text{ min}^{-1}$. The morphology was examined with a Nova NanoSEM-450 field emission scanning electron microscopy (FESEM). Prior to the beginning, the sample was sprayed on platinum-coated stainless steel substrate. UV-vis absorption of coordination compound solution was measured by a T6 New-century ultraviolet and

visible spectrophotometer with DI water as a baseline against background. Thermogravimetric and differential scanning calorimetry (TG-DSC) analysis of the synthesized powders was carried out on a TA Q600 thermal gravimetric analyzer. The experiment was performed in atmosphere from room temperature to 800 °C with a heating rate of 10 °C min⁻¹, using alumina as reference and 5–10 mg of sample.

The surface area of spinel CoMn₂O₄ hollow spheres was determined by nitrogen adsorption and desorption measurements at liquid nitrogen temperature using 3 Flex multi-purpose gas adsorption instrument. Prior to adsorption, the sample was degassed in vacuum at 200 °C for 4 h. Specific surface area was calculated from the Brunauer-Emmett-Teller (BET) method and main pore size was analyzed with Barrett-Joyner-Halenda (BJH) method. The element contents of Co and Mn were detected with an inductively coupled plasma atomic emission spectrometer (ICP-AES, Agilent, 167 nm–785 nm/725). X-ray photoelectron spectroscopy (XPS) was performed on an ESCALAB 250Xi (Thermo Fisher) apparatus with Al K α X-rays radiation to analyze the surface oxidation state distribution of the elements in the sample. H₂ temperature programmed reduction (H₂-TPR) experiments were carried out on an AutoChem II 2920 V4.05 apparatus. The samples were reduced using 10% H₂/Ar (v/v) mixed gas with a flow of 30 mL/min at a heating rate of 10 °C min⁻¹.

2.3. The selective oxidation of HMF

As a general procedure, the selective oxidation of HMF was performed in a stainless-steel autoclave equipped with an internal thermostat under a magnetic stirring. Typically, 50 mg of catalyst, 63 mg of HMF and 5 g of DMF as solvent were added into the reactor. The air in the reactor was replaced with O₂ by purged 3 times and kept the O₂ pressure at 0.75 Mpa at room temperature. When the mixture was heated to the desired temperature, the pressure was controlled at 0.8 MPa and maintained a specific reaction time. All the changes of reaction parameters: temperature, amount of the catalysts or reaction time were notified. Finally, the autoclave was cooled down to room temperature by quenching with cold water.

The reaction supernatant solution was analyzed using LC-2010AHT SHIMADZU liquid chromatograph equipped with a UV–vis detector and Benson polymeric BP-OA column. The mobile phase consisted of H₂SO₄ with pH = 3, at a flow rate of 0.8 mL min⁻¹, and the analysis was carried out at 45 °C, using an injection volume of 1 μ L. HMF conversion and DFF selectivity were calculated based on external calibration curves using five individual samples.

3. Results and discussion

3.1. Formation of spinel CoMn₂O₄ hollow spheres

The preparation of spinel CoMn₂O₄ hollow spheres involves the solution synthesis of uniform metal glycerate solid spheres and subsequent thermal annealing in air to remove coordinated organic ligands. In the first step, uniform cobalt-manganese glycerate (Co/Mn-Gly) spheres as the precursor (Fig. 2) was prepared by a facile solvothermal method. There is a strong peak at around 10° ascribing to the formation of metal alkoxide by alcoholysis and coordination of glycerol with the metal ions. The crystalline of the precursor obtained from solvothermal reaction is particularly similar to reported Ni/Co-glycerate [30] and Fe-glycerate [31]. The metal ions form coordination compounds with organic ligands, which crystallizes in Co/Mn-Gly under the solvothermal conditions. The Co/Mn-Gly solid spheres can be readily converted to spinel CoMn₂O₄ hollow spheres by a simple non equilibrium heat treatment via removal of coordinated organic ligands. All diffraction peaks of the sample after calcination can be indexed to CoMn₂O₄ (JCPDS 01-1126), a typical spinel structure, where Co²⁺ and Mn³⁺ separately occupy tetrahedral A and octahedral B sites. Besides, no other impurity diffraction peaks are observed, implying the high

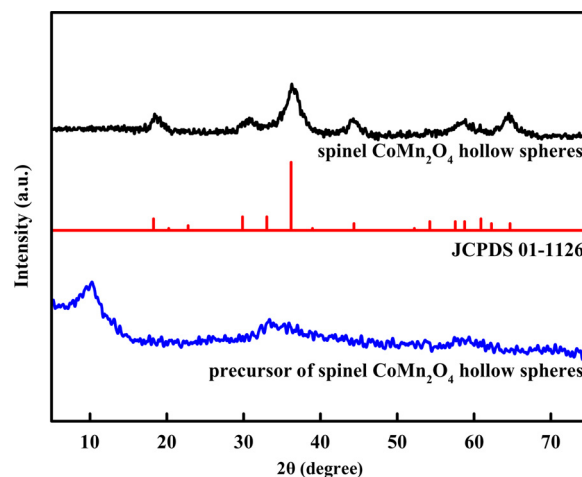


Fig. 2. XRD patterns of CoMn₂O₄ precursor and spinel CoMn₂O₄ hollow spheres.

purity of the product.

The final morphology of the spinel CoMn₂O₄ hollow spheres was characterized by FESEM. As shown in Fig. 3, the spinel CoMn₂O₄ is composed of uniform microspheres with diameters of 3.5 ± 0.5 μ m and the morphology could be perfectly preserved after calcination without severe cracking. The surface of the sphere in Fig. 3b is a bit rough and cracking due to the loss of glycerol ligand during calcination, while there is a cavity inside with relative small diameters of the particles (Fig. 3c), demonstrating the formation of hollow structure. Similar Ni/Co oxides and Fe₃O₄ hollow spheres have been reported previously [30,31]. However, there is no spheres formed without addition of glycerol in the preparation (see Fig. 3d). The material is composed of granules with diameter of 1 μ m accumulated by the irregular, amorphous, and rough particles. The results demonstrate the important and indispensable role of glycerol for the formation of hollow sphere structure during solvothermal synthesis.

In order to explore the possible fabrication process of spinel CoMn₂O₄ hollow spheres, UV–vis adsorption spectra of different precursor solutions are shown in Fig. 4. It is acceptable that d-d ligand field transition happens for the d orbitals of transition metal ions under the action of ligand, which can be used for the qualitative analysis of complex structure by the migration of UV–vis absorption peaks. To achieve a better understanding of offset, the solution was diluted with different proportions of IPA. There is no absorption peak of IPA and Gly, while an absorption peak of M²⁺ (M = Co²⁺ and Mn²⁺) in IPA appears at 526 nm, indicating the formation of M-IPA coordination compound. After the addition of glycerol, the absorption peak leading to a blue shift to the wavelength of 518 nm results from the formation of new M-Gly coordination compound, where -IPA is replaced by -Gly. When IPA and H₂O coexist in system, the absorption peak continually shifts to 511 nm, which stems from a red shift of M²⁺ in water. While an absorption wavelength at 508 nm ascribes to hydration effect between M²⁺ and water, which has been confirmed by water structure around metal ions [32]. The red shift of hydrated M²⁺ and blue-shifted M-Gly is that H₂O strongly interacts with IPA and M²⁺ via hydrogen bond interaction and it finally forms -M-Gly-H₂O- coordination compounds.

Based on the discussion above, the preparation process of spinel CoMn₂O₄ hollow spheres is as following (Fig. 5). Firstly, M-IPA coordination complexes were generated due to complexation reaction between Co²⁺, Mn²⁺, and IPA, where -IPA was formed by isopropanol dehydrogenation. Then, -IPA was replaced by -Gly because of M-IPA poor dynamical stability [31]. Simultaneously, Co/Mn-Gly-H₂O coordinated complex was formed owing to the added H₂O also combined with Gly and M²⁺ through hydrogen bond. Under solvothermal

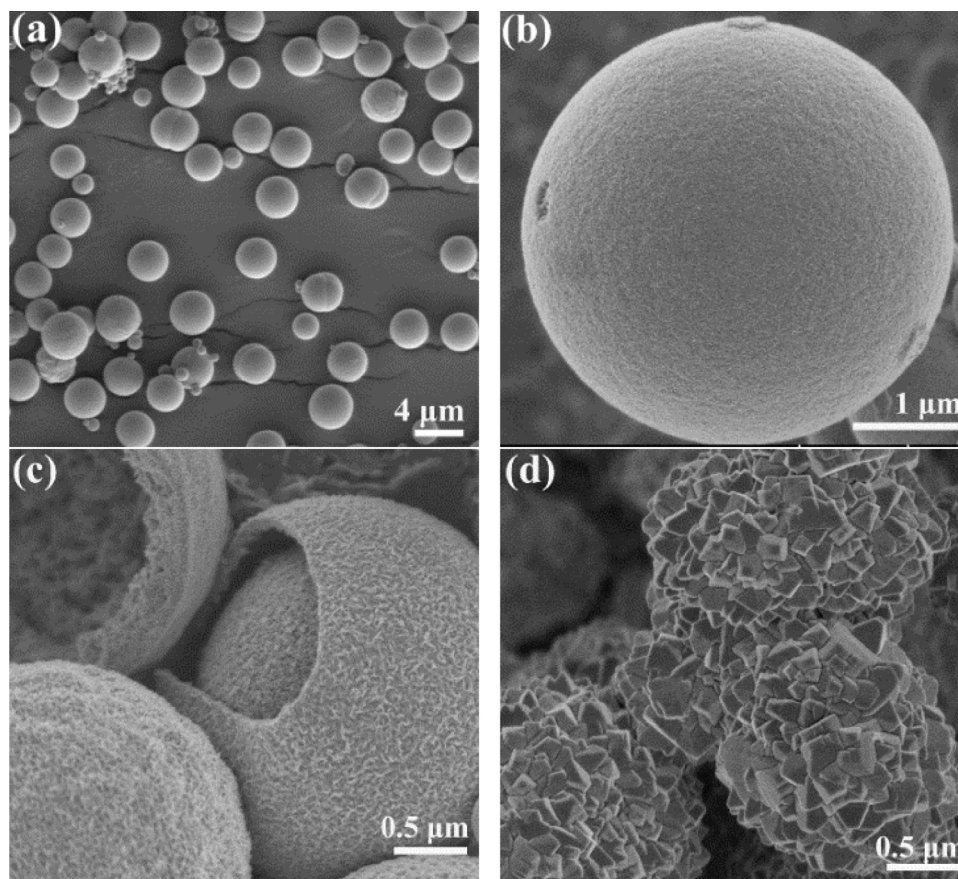


Fig. 3. FESEM images of spinel CoMn_2O_4 hollow spheres (a–c) with and (d) without glycerol addition.

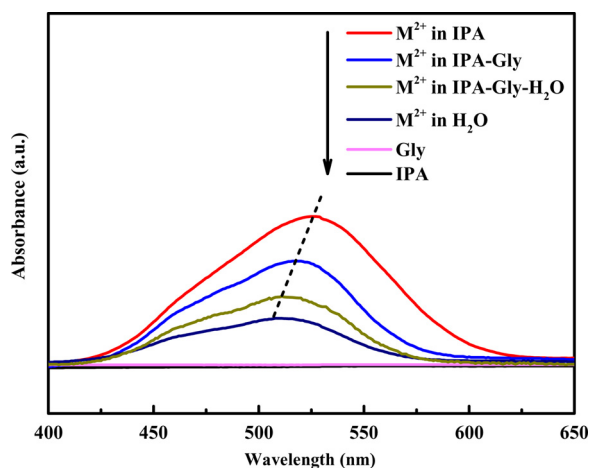


Fig. 4. UV-vis adsorption spectra of different precursor solutions.

environment, $-\text{Co/Mn-Gly-H}_2\text{O}-$ connecting each other will gradually aggregate into hierarchical spheres through dehydration and alcohol-oxygen groups driven by the minimization of interfacial energy, leading to formation of Co/Mn-Gly by the heterogeneous nucleation process. Finally, the release of glycerol ligand was caused by calcination in air and Co/Mn-Gly spheres converted into high crystalline spinel CoMn_2O_4 hollow spheres by a simple nonequilibrium treatment process.

3.2. Characterization of spinel CoMn_2O_4 hollow spheres

The spinel CoMn_2O_4 hollow spheres were successfully prepared by solvothermal method combined with calcination of Co/Mn-Gly

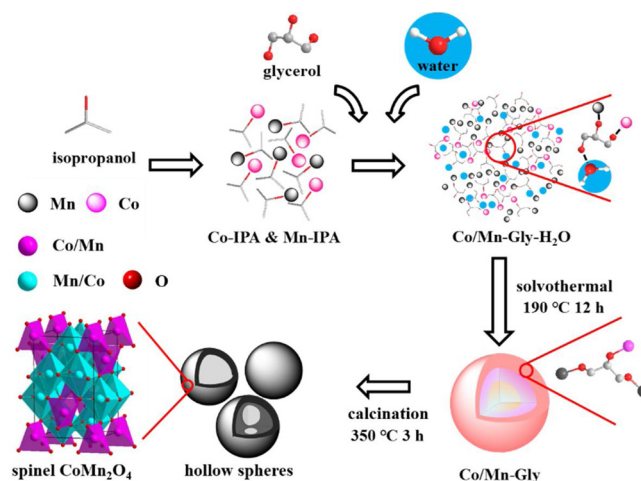


Fig. 5. Schematic illustration of the formation process of spinel CoMn_2O_4 hollow spheres.

precursor. There are two-stage mass loss from room temperature to $800\text{ }^\circ\text{C}$ in air through thermogravimetric analysis (TGA) of CoMn_2O_4 precursor as shown in Fig. 6. The weight loss at stage I below $200\text{ }^\circ\text{C}$ is 5.1%, which is attributed to the release of physically adsorbed water on the surface, trapped in the pores and interlayer space. The stage II appeared from $200\text{ }^\circ\text{C}$ to $300\text{ }^\circ\text{C}$ with a 37.6% weight loss corresponding to a sharp DSC exothermic peak can be ascribed to the decomposition of glycerol ligand in the precursor, as confirmed by XRD recorded before and after calcination. It demonstrates the decomposition of the CoMn_2O_4 precursor starts from around $200\text{ }^\circ\text{C}$ and completes at around $300\text{ }^\circ\text{C}$. According to the TGA and DSC curves, it is reasonable that a

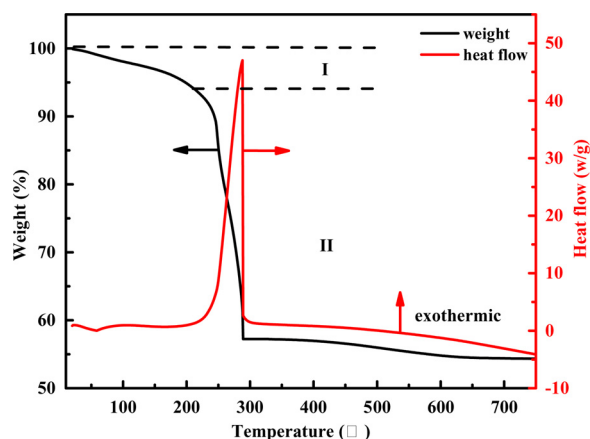


Fig. 6. TGA and DSC curves of as-prepared Co/Mn-glycerate precursor.

calcined temperature of 350 °C was chosen for thermal treatment of the precursor to ensure its complete decomposition.

The spinel CoMn_2O_4 hollow spheres were further characterized by nitrogen adsorption/desorption at -196 °C (see Fig. 7). The isotherms are of type IV isotherms with a distinct H2-type hysteresis loop in the P/P₀ region from 0.45 to 0.99, which does not close until the saturation pressure is reached. The Brunauer-Emmett-Teller (BET) method was used to calculate surface area and the corresponding Barrett-Joyner-Halenda (BJH) formula was employed to evaluate the pore distribution using the desorption branch of the isotherm curve. The BET surface area is estimated to be $82.6 \text{ m}^2 \text{ g}^{-1}$ and the BJH calculation gives a main pore size distribution ranging from 3 to 10 nm (inset of Fig. 7). Thus, the porous spinel CoMn_2O_4 hollow spheres are beneficial for oxidation reaction during the charging/discharging products and expect to improve catalytic activity [33].

The spinel structure of CoMn_2O_4 hollow spheres with different Co/Mn molar ratios were also taken into consideration. The XRD patterns of different spinel CoMn_2O_4 hollow spheres, sole Mn_3O_4 and Co_3O_4 are shown in Fig. 8. The diffraction peaks of both Mn_3O_4 and Co_3O_4 prepared are perfectly associated to JCPDS No. 24-0734 and JCPDS No. 43-1003, respectively. Sharp peaks observed are indicative of highly crystallized grains. Mn_3O_4 containing both di- and tri-valent manganese belongs to body-centered tetragonal spinel (space group I41/adm), while Co_3O_4 similar to Mn_3O_4 is indexable to the face-centered cubic spinel (space group Fd-3 m). Compared with Mn_3O_4 and Co_3O_4 , the diffraction peaks of spinel CoMn_2O_4 with different Co/Mn molar ratios can be assigned to different spinel structures. There is a phase transitions for $\text{Co}_x\text{Mn}_{3-x}\text{O}_4$ ($0 \leq x \leq 3.0$) depending on the x values. It

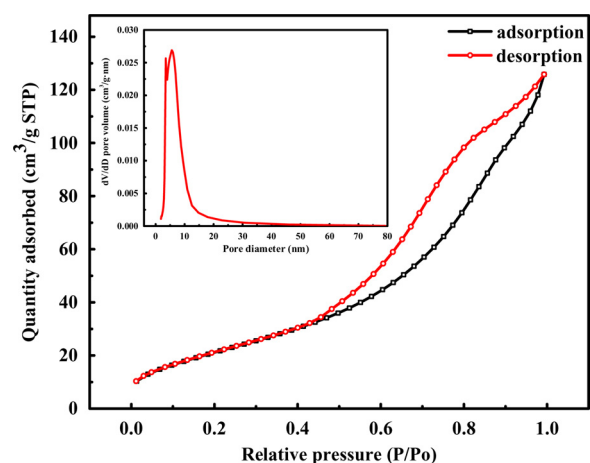


Fig. 7. Nitrogen adsorption/desorption isotherms and pore size distribution plots (inset) of the spinel CoMn_2O_4 hollow spheres.

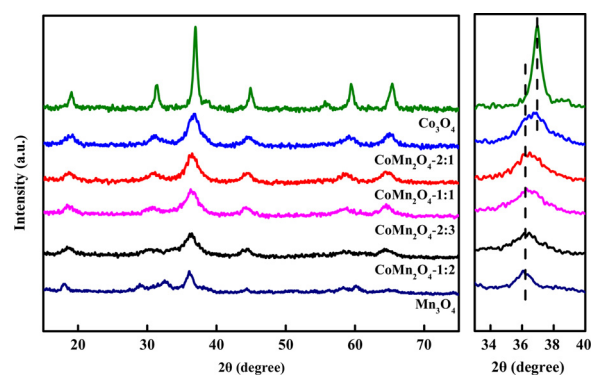


Fig. 8. XRD patterns of spinel CoMn_2O_4 hollow spheres with different Co/Mn molar ratios.

crystallizes in a body-centered tetragonal structure between $0 < x < 1.6$ and a face-centered cubic form between $1.6 < x < 3.0$ [34].

For spinel CoMn_2O_4 hollow spheres, Co^{2+} and Mn^{3+} are separately occupy tetrahedral and octahedral sites of the spinel structure, which ascribes to body-centered tetragonal spinel (space group I41/adm, JCPDS No. 01-1126). As Co/Mn ratio in precursor increases, the peak positions of CoMn_2O_4 obviously shifts to high 2θ values. The shift of 2θ values indicates that a part of Mn atom locations in lattice is occupied by smaller Co atom ($r_{\text{Mn}^{3+}} = 0.645 \text{ \AA}$, $r_{\text{Co}^{2+}} = 0.545 \text{ \AA}$), which results in decrease in the lattice parameter. The decreased lattice constants of tetrahedral crystallites are 5.7567, 5.7283, and 5.6953 Å for CoMn_2O_4 with Co/Mn ratios of 1:2, 2:3, and 1:1, respectively, based on measured XRD patterns. On the other hand, with increased Co/Mn ratio to 2, the prepared material undergo characteristic structural changes, which are a consequence of the Co and Mn cations exchanging their lattice sites under the bottom-up solvothermal process. Thus, it is identical to face-centered cubic Co_3O_4 phase, where the octahedral and tetrahedral sites are occupied exclusively by Co and Mn cations. Therefore, the prepared spinel Co-Mn-O phases correspond to a class of configuration rather than a single crystallographic structure, which matches well with XRD results and previous reports [34,35].

XPS was used to monitor the oxidation states of spinel CoMn_2O_4 -2:3 and the results are shown in Fig. 9. All of the binding energies were corrected for specimen charging by referencing them to the C 1s peak at 284.4 eV. The peaks of Co, Mn, O and C elements have been observed in the scan survey spectrum (Fig. 9a). Due to the Co $2p_{3/2}$ binding energy of Co^{2+} is close to that of Co^{3+} , the Co $2p_{3/2}$ spectrum of the sample is fitted into two peaks of Co^{2+} , Co^{3+} , and a shakeup satellite above the main $2p_{3/2}$ line by a Gaussian fitting method (Fig. 9b). The peak at 780.3 eV is assigned to Co^{2+} and the peak at 781.6 eV is attributed to Co^{3+} [36]. In the Mn $2p_{3/2}$ spectrum (Fig. 9c), three peaks observed at 641.3, 642.8, and 645.1 eV are assigned to Mn^{2+} , Mn^{3+} , and Mn^{4+} , respectively [37]. It indicates the CoMn_2O_4 -2:3 definitely coexists mixed phases, which is in good agreement with the molar ratio of Co and Mn during the prepared process. As shown in Fig. 9d, the O 1s spectrum is fitted into two peaks at 530.1 and 531.3 eV, which are attributed to metal-oxygen bonds and defect sites with low oxygen coordination [38]. The low oxygen coordination with vacancies plays an important role in the improving mobility of oxygen and favors oxygen transfer on the surface of catalysts [38,39], which makes spinel CoMn_2O_4 hollow spheres improving catalytic activity for oxidation reactions.

3.3. Catalytic activities of spinel CoMn_2O_4 hollow spheres

It is generally accepted that the conversion of HMF and selectivity of DFF were extremely sensitive to the reaction temperature [40]. In order to obtain high HMF conversion and DFF selectivity, the reaction

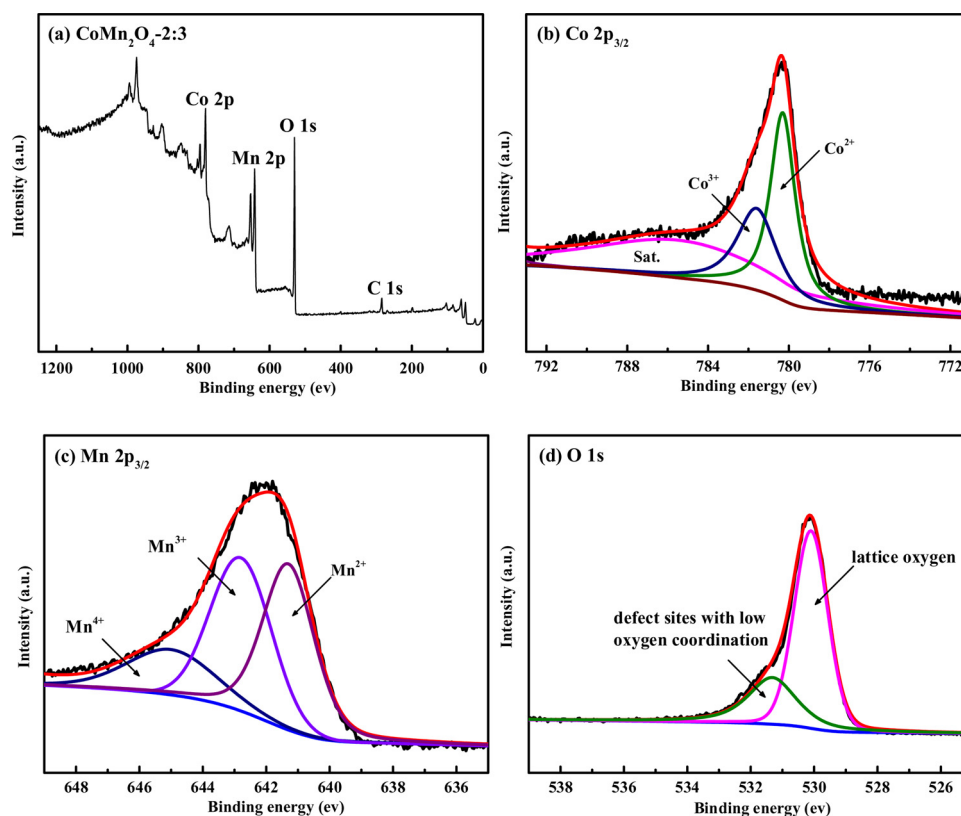


Fig. 9. (a) Wide survey XPS spectrum, high-resolution XPS spectra (b) Co $2p_{3/2}$, (c) Mn $2p_{3/2}$, and (d) O $1s$ of as-synthesized $\text{CoMn}_2\text{O}_4\text{-}2:3$.

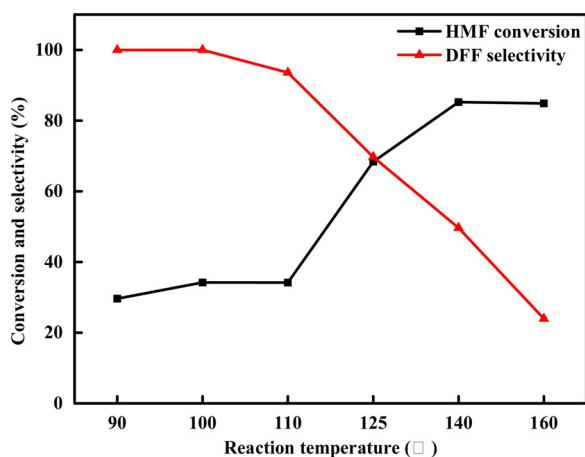


Fig. 10. Influence of reaction temperature on HMF oxidation.

temperature of HMF oxidation was optimized, while other reaction conditions maintained constant such as catalyst amount, reaction pressure and time, etc. (Fig. 10). The higher the reaction temperature is, the higher HMF conversion can be obtained. The HMF conversion is only 29.6% at 90 °C, while greatly increases to 84.9% with reaction temperature at 160 °C. According to molecular dynamics theory, more molecules are in contact with catalyst active sites at higher reaction temperatures due to the more intense molecular thermal motion [41]. Besides HMF conversion, the selectivity to DFF is also greatly affected by the reaction temperature and decreases with the increased reaction temperature. It is close to 100% at reaction temperature less than 100 °C. However, DFF selectivity decreases to 24.0% further raising the temperature up to 160 °C. On the one hand, the instability of HMF at high temperature results in by-products such as ether, ketone, ester, and water generated by aldol condensation reactions between parts of

reactants. On the other hand, ring-open reaction occurs and produces levulinic acid and insoluble humin [42,43]. Therefore, it can be deduced that 100 °C should be the optimized reaction temperature in this process.

For the sake of comparison, the catalytic activities of different catalysts are shown in Table 1. A moderate HMF conversion of 30.6% along with ca. 100% selectivity to DFF is obtained for prepared Mn_3O_4 hollow spheres, while commercial Mn_3O_4 with BET surface area of $5\text{--}7\text{ m}^2\text{ g}^{-1}$ only gives HMF conversion of 1.0% (Table 1, entries 1–2). Previous reports on 3D NiO hollow spheres and $\text{CeO}_2/\text{Al}_2\text{O}_3$ hollow fibers demonstrate that hollow structures with more BET surface areas can provide more active sites and diffusion pathways for absorbing more reactants, resulting in enhanced bio and adsorption properties [44,45]. Herein, the hollow Mn_3O_4 spheres with exposed more active sites than commercial one significantly improves its catalytic performance. Additionally, oxidized product DFF can fast leave the catalyst surface leading to high selectivity, avoiding further oxidation.

Single Co_3O_4 with poor catalytic performance (Table 1, entry 7)

Table 1
Different Co-Mn catalysts for HMF oxidation^a.

Entry	Catalysts	HMF conversion (%)	Selectivity(%)		
			DFF	FFCA	Others
1	Mn_3O_4 -commercial	0.9	–	–	100
2	Mn_3O_4	30.6	> 99	–	–
3	$\text{CoMn}_2\text{O}_4\text{-}1:2$	34.2	> 99	–	–
4	$\text{CoMn}_2\text{O}_4\text{-}2:3$	41.6	> 99	–	–
5	$\text{CoMn}_2\text{O}_4\text{-}1:1$	33.7	> 99	–	–
6	$\text{CoMn}_2\text{O}_4\text{-}2:1$	36.0	92.1	5.2	2.6
7	Co_3O_4	6.2	69.9	20.9	9.2
8	$\text{Co}_3\text{O}_4\text{-Mn}_3\text{O}_4\text{-}2:3$	33.7	> 99	–	–

^a Reaction conditions: 0.5 mmol HMF, 5 g DMF, 50 mg catalyst, 0.8 MPa O_2 , 100 °C, 2 h.

demonstrates it is not active in this reaction, but it can efficiently promote Mn_3O_4 catalyst with enhanced catalytic activity. When Co/Mn binary oxides are used, the catalytic activities improve obviously (Table 1, entries 3–6). Furthermore, the catalytic activities initially increase to the maximum HMF conversion (41.6%) and 100% selectivity to DFF, and then decrease with the increasing of Co/Mn ratios. The HMF conversion decreases to 36.0% and DFF selectivity is down to 92.1% with continually increased Co/Mn ratio to 2:1. As seen in entries 2 and 7, Mn_3O_4 hollow spheres is active, while Co_3O_4 can just promote the reaction. Therefore, excessive Co replaces Mn lattice sites in the spinel CoMn_2O_4 hollow spheres, which may reduce the amounts of active Mn species and result in the decrease of catalytic performance. The similar results have been reported by previous works for the selective oxidation of HMF into DFF [46,47].

It is reported manganese oxides exhibit moderate catalytic performance for the selective oxidation into DFF [47]. After the addition of Co ($(\text{NO}_3)_2 \cdot 6\text{H}_2\text{O}$ as Co source during the preparation, there is a synergistic effect between Co and Mn species in binary oxides, which leads to significant improvement in catalyst performance. When the Co/Mn ratio is 1:2 forming spinel CoMn_2O_4 hollow spheres, HMF conversion is 34.2% and DFF selectivity is 100%, indicating synergistic effect of Co and Mn species of spinel CoMn_2O_4 hollow spheres. When Co_3O_4 and Mn_3O_4 were mixed through conventional mechanical mean with a Co/Mn ratio of 2:3 ($\text{Co}_3\text{O}_4\text{-Mn}_3\text{O}_4\text{-2:3}$, Table 1, entry 8), it is found that $\text{Co}_3\text{O}_4\text{-Mn}_3\text{O}_4\text{-2:3}$ shows very similar catalytic performance to Mn_3O_4 (Table 1, entry 2), and significantly lower than that of $\text{CoMn}_2\text{O}_4\text{-2:3}$. These results indicate that the high catalytic performance of $\text{CoMn}_2\text{O}_4\text{-2:3}$ maybe due to the synergistic effect between Co and Mn species in the spinel CoMn_2O_4 hollow spheres, rather than physical contact. In brief, the selective oxidation of HMF to DFF catalyzed by Co-Mn-O is a single-electron-transfer process. The CoMn_2O_4 system exhibits high catalytic activity maybe due to the formation of heteronuclear cluster complexes CoMn_2O_4 , which affects and promotes the electron-transfer process [48,49].

ICP-AES results make it clear that Co/Mn ratios are similar to those added in the preparation. $\text{CoMn}_2\text{O}_4\text{-2:3}$ remaining spinel phase demonstrate excessive Co species highly dispersed or incorporated into CoMn_2O_4 lattice exhibiting the strongest synergistic effect, resulting in the highest catalytic performance. However, further increase in Co content to Co/Mn ratio of 1, $\text{CoMn}_2\text{O}_4\text{-1:1}$ shows a decreased HMF conversion (33.7%) and high selectivity (> 99%). The high concentrated Co species means low amounts of active Mn species, which leads to decreased catalytic activity. When Co/Mn ratio continually increases to 2, $\text{CoMn}_2\text{O}_4\text{-2:1}$ reveals 36.0% HMF conversion as well as a decreased selectivity to DFF (92.1%). Here, $\text{CoMn}_2\text{O}_4\text{-2:1}$ with face-centered cubic Co_3O_4 phase, which should affect the original active sites of Mn, results in decreased DFF selectivity. It is also supported by the poor catalytic activity of Co_3O_4 with low selectivity (Table 1, entry 7).

To further substantiate the effects of Co/Mn molar ratios on the catalytic activity, the H_2 -TPR profiles of different spinel CoMn_2O_4 hollow spheres, Mn_3O_4 , and Co_3O_4 are shown in Fig. 11. Two obvious reduction peaks in the reduction profile of Mn_3O_4 are observed. The low-temperature peak at 220 °C is attributed to the reduction of Mn^{4+} species dispersed on Mn_3O_4 and the high-temperature peak at 362 °C is due to the typical reduction of Mn_3O_4 to MnO [50]. The Mn^{4+} species has been confirmed by the Mn 2p_{3/2} spectrum. In the case of Co_3O_4 , the reduction peak at 225 °C is ascribed to the reduction of Co_3O_4 to CoO , and the peak around 240–255 °C is due to the transformation of CoO to Co^0 [51]. Obviously, the reduction temperatures of all pinel CoMn_2O_4 hollow spheres are lower than Mn_3O_4 and Co_3O_4 , implying higher oxygen mobility in the spinel CoMn_2O_4 hollow spheres. The reduction peak around 200 °C is attributed to the reduction of Mn^{4+} species to Mn_3O_4 in spinel CoMn_2O_4 and the appearance of peak around 290 °C is due to the reduction of Mn_3O_4 to MnO and Co_3O_4 to CoO [36].

In particular, the reduction peak of CoO to Co^0 for CoMn_2O_4 was

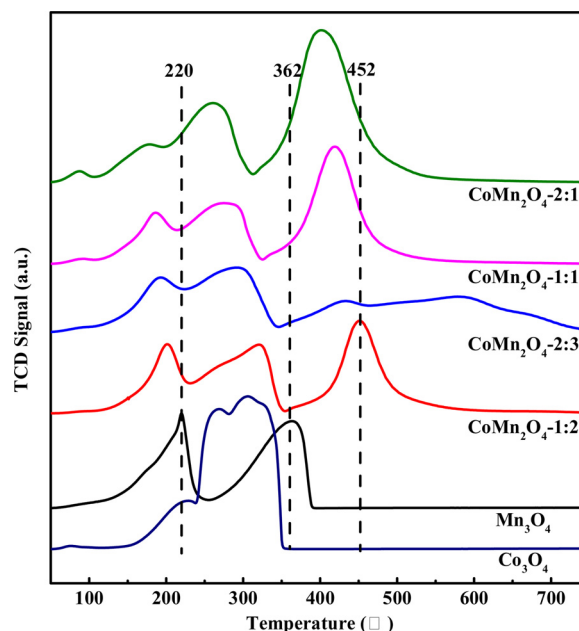


Fig. 11. H_2 -TPR profiles of spinel CoMn_2O_4 with different Co-Mn ratios.

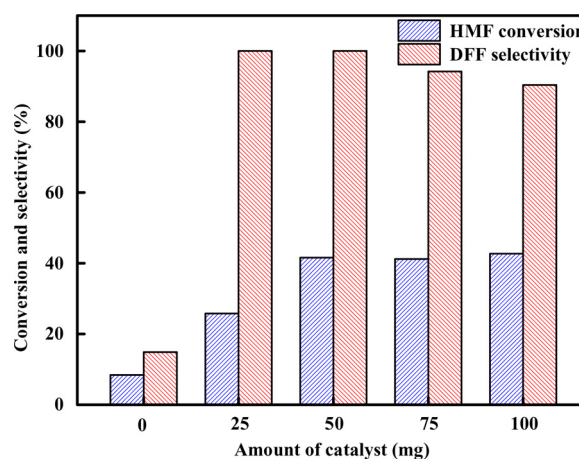


Fig. 12. Influence of catalyst amount for selective aerobic oxidation of HMF.

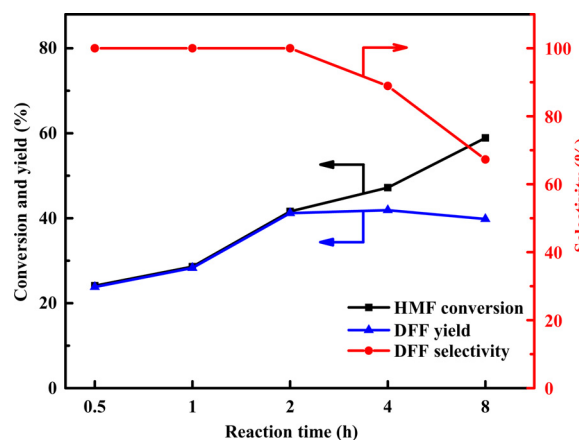


Fig. 13. Time course study of HMF oxidation with spinel CoMn_2O_4 hollow spheres.

obtained around 450 °C, which shifts to higher temperature attributing to a synergistic effect between Co and Mn in the spinel CoMn_2O_4 hollow spheres [36,51]. On the contrary, the reduction peaks of Mn^{4+} , Mn_3O_4 ,

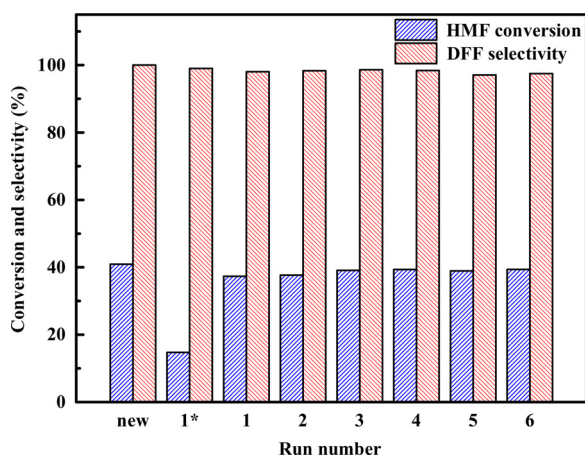


Fig. 14. Recyclability experiments with spinel CoMn_2O_4 hollow spheres for the selective oxidation of HMF into DFF.

and CoO have obvious shifts to lower temperatures with the addition of Co species, implying that synergistic effect between Co and Mn improves the oxygen mobility and reducibility in the spinel CoMn_2O_4 [52]. Therefore, spinel CoMn_2O_4 catalysts have better catalytic activities than those of Mn_2O_3 and Co_3O_4 , which are well agreed with the results in Table 1. In addition, the peak areas indicate hydrogen consumption amounts and the lowest reduction peak area of different spinel CoMn_2O_4 illustrates the reduction capacity of the same reduction process [53]. It is found that the peak area ratios of the lowest reduction peak obtained by integration are 2:2:1.4:1 for spinel CoMn_2O_4 with Co/Mn ratios of 1:2, 2:3, 1:1, and 2:1. According to the reducibility tested by H_2 -TPR profiles, spinel CoMn_2O_4 -2:3 shows both the maximum reduction peak area and the lowest reduction temperature. Therefore, it possess the maximum amount of mobile oxygen species to be adsorbed and further generate active oxygen species, which would be involved in the reaction. As a result, the CoMn_2O_4 -2:3 with the highest reduction amount of Mn^{4+} and the lowest reduction peak shows the best performance, as shown in Table 1.

Aerobic oxidation of HMF to DFF was also carried out to study the effects of amounts of spinel CoMn_2O_4 hollow spheres. As shown in Fig. 12, there is only about 8.0% HMF conversion with 14.9% selectivity to DFF in the absence of spinel CoMn_2O_4 hollow spheres due to self-polymerization of HMF. With the addition of 25 mg of the CoMn_2O_4 -2:3 catalysts, the catalytic performance significantly improves, however the active sites are not sufficient to activate the substrate. When the catalyst amount increases to 50 mg, 41.6% conversion of HMF and ca. 100% selectivity of DFF are obtained. The more the catalytic amount, the more active sites are provided, the more HMF is converted in the reaction. Thus the HMF conversion increases and DFF selectivity is up to 100%. HMF conversion maintains constant, but DFF selectivity shows a downward trend with a continual increase in catalyst amount. It is the fact that excessive catalyst amount provides too many active sites, which not only catalyzes the selective aerobic oxidation of HMF to DFF, but further oxidizes DFF into other products, such as 5-formylfuroic acid, 2,5-furandicarboxylic acid, and so on.

The influence of reaction time on the conversion of HMF and selectivity to DFF is studied with the CoMn_2O_4 -2:3 catalyst as shown in Fig. 13. The HMF conversion is about 24.1%, 28.6%, and 41.6% in 0.5, 1, and 2 h of reaction time together with selectivity to DFF about 100%, respectively. The longer the reaction time is, the more HMF is converted in the reaction and the conversion increases. With prolonged reaction time, the conversion of HMF increases gradually to 47.2% (4 h) and 58.9% (8 h) while selectivities to DFF decreases sharply to 88.9% and 67.3%, respectively. It needs to be pointed out that the yield of DFF is retained by improving reaction time from 2 to 8 h. The main reason for the reduction of DFF selectivity is side reaction occurs such as HMF

polymerization or cracking [43]. Simultaneously, a small amount of DFF is further oxidized into FFCA and other products, resulting in the decreased selectivity of DFF.

Catalyst recycling is of great importance in the field of heterogeneous catalysis. The reusability and stability of spinel CoMn_2O_4 hollow spheres was investigated in six successive consecutive runs for the selective oxidation of HMF into DFF with the same conditions. After each reaction, the catalyst was dried at 70 °C for 10 h after being washed with ethanol more than three times, and then calcined at 350 °C for 3 h before reused. For comparison, another catalyst without thermal treatment (1*) was also performed for the reaction. As shown in Fig. 14, the HMF conversion of 1* seriously declines to 14.8%, probably owing to the substrate accumulated on the catalyst surface. On the contrary, both HMF conversion and DFF selectivity of the catalysts after calcined only decrease about 2% after six runs, demonstrating that the spinel CoMn_2O_4 hollow spheres are highly stable during the selective oxidation of HMF to DFF and the catalytic activity can be recovered well by calcination.

4. Conclusion

In summary, cost-effective spinel CoMn_2O_4 hollow spheres have been prepared by a solvothermal method and the self-assembly formation processes were detailed studied. The as-prepared CoMn_2O_4 hollow spheres system exhibited high catalytic activity for the selective oxidation of HMF into DFF in comparison with single metal oxide. Particularly, CoMn_2O_4 hollow spheres with Co/Mn molar ratio of 2/3 showed the highest catalytic performance with 41.6% HMF conversion and 100% DFF selectivity due to the strong synergistic effect of metal oxides between Mn and Co species. In addition, the catalyst could be readily reused without significant loss of its catalytic activity. Thus, the spinel CoMn_2O_4 hollow spheres with superior catalytic activity for the selective oxidation of HMF are expected to be useful in many other applications.

References

- [1] A.A. Rosatella, S.P. Simeonov, R.F.M. Frade, C.A.M. Afonso, *Green Chem.* 13 (2011) 754–793.
- [2] M.J. Climent, A. Corma, S. Iborra, *Green Chem.* 16 (2014) 516–547.
- [3] X. Li, Y. Zhang, *Green Chem.* 18 (2016) 643–647.
- [4] D.M. Alonso, J.Q. Bond, J.A. Dumesic, *Green Chem.* 12 (2010) 1493–1513.
- [5] G. Yong, Y. Zhang, J.Y. Ying, *Angew. Chem. Int. Ed.* 47 (2008) 9345–9348.
- [6] C.T. Chen, C.V. Nguyen, Z.Y. Wang, Y. Bando, Y. Yamauchi, M.T.S. Bazziz, A. Fatehmulla, W.A. Farooq, T. Yoshikawa, T. Masuda, K.C.W. Wu, *ChemCatChem* 10 (2018) 361–365.
- [7] J. Ma, Z. Du, J. Xu, Q.H. Chu, Y. Pang, *ChemSusChem* 4 (2011) 51–54.
- [8] M. Shaikh, S.K. Singh, S. Khilari, M. Saha, K.V.S. Ranganatha, *Catal. Commun.* 106 (2018) 64–67.
- [9] K.R. Vuyyuru, P. Strasser, *Catal. Today* 195 (2012) 144–154.
- [10] Y.Q. Zhu, M.N. Shen, Y.G. Xia, M. Lu, *Catal. Commun.* 64 (2015) 37–43.
- [11] G.D. Yadav, R.V. Sharma, *Appl. Catal. B Environ.* 147 (2014) 293–301.
- [12] K. Ghosh, R.A. Molla, M.A. Iqbal, S.S. Islama, S.M. Islam, *Appl. Catal. A Gen.* 520 (2016) 44–52.
- [13] Z.Y. Gui, W.R. Cao, S. Saravanamurugan, A. Riisager, L.F. Chen, Z.W. Qi, *ChemCatChem* 8 (2016) 3636–3643.
- [14] Z.Z. Yang, W. Qi, R.X. Su, Z.M. He, *ACS Sustain. Chem. Eng.* 5 (2017) 4179–4187.
- [15] S. Biswas, B. Dutta, A. Mannodi-Kanakkithodi, R. Clarke, W.Q. Song, R. Ramprasadc, S.L. Suib, *Chem. Commun.* 53 (2017) 11751–11754.
- [16] I. Sádaba, Y.Y. Gorbanev, S. Kegnæs, S.S.R. Putluru, R.W. Berg, A. Riisager, *ChemCatChem* 5 (2013) 284–293.
- [17] F. Neatu, N. Petrea, R. Petre, V. Somoghi, M. Florea, V.I. Parvulescu, *Catal. Today* 278 (2016) 66–73.
- [18] D.X. Martínez-Vargas, J.R.D.L. Rosa, L. Sandoval-Rangel, J.L. Guzmán-Mara, M.A. Garza-Navarro, C.J. Lucio-Ortiz, D.A.D.H. Ríoa, *Appl. Catal. A Gen.* 547 (2017) 132–145.
- [19] L.M. Ning, S.Y. Liao, Y.F. Sun, L.H. Yu, X.L. Tong, *Waste Biomass Valori.* 9 (2018) 95–101.
- [20] B.Y. Lin, Y. Liu, L. Heng, J. Ni, J.X. Lin, L.L. Jiang, *Catal. Commun.* 101 (2017) 15–19.
- [21] Y. Cao, Z. Xing, M. Hu, Z.Z. Li, X.Y. Wu, T.Y. Zhao, Z.Y. Xiu, S.L. Yang, W. Zhou, *J. Catal.* 356 (2017) 246–254.
- [22] Z. You, Y. Su, Y. Yu, H. Wang, T. Qin, F. Zhang, Q.H. Shen, H. Yang, *Appl. Catal. B Environ.* 213 (2017) 127–135.

- [23] Y. Cheng, Z. Li, Y. Li, S.S. Dai, G.B. Ji, H.Q. Zhao, J.M. Cao, Y.W. Du, *Carbon* 127 (2018) 643–652.
- [24] Y. Cheng, J.M. Cao, Y. Li, Z.Y. Li, H.Q. Zhao, G.B. Ji, Y.W. Du, *ACS Sustain. Chem. Eng.* 6 (2018) 1427–1435.
- [25] L. Wu, Y. Hu, X. Zhang, J.Q. Liu, X. Zhu, S.K. Zhong, *J. Power Sources* 374 (2018) 40–47.
- [26] Y. Yi, G.H. Lee, J.C. Kim, H.W. Shim, D.W. Kim, *Chem. Eng. J.* 327 (2017) 297–306.
- [27] S.C. Cai, Z.H. Meng, H.L. Tang, Y. Wang, P. Tsiakarasc, *Appl. Catal. B Environ.* 217 (2017) 477–484.
- [28] Z. Huang, H.Y. Pan, W.J. Yang, H.H. Zhou, N. Gao, C.P. Fu, S.C. Li, H.X. Li, Y.F. Kuang, *ACS Nano* 12 (2018) 208–216.
- [29] L. Yu, H. Hu, H.B. Wu, X.W. Lou, *Adv. Mater.* 29 (2017) 1604563–1604602.
- [30] L.F. Shen, L. Yu, X.Y. Yu, X.G. Zhang, X.W. Lou, *Angew. Chem. Int. Ed.* 54 (2015) 1868–1872.
- [31] F.X. Ma, H. Hu, H.B. Wu, C.Y. Xu, Z.C. Xu, L. Zhen, X.W. Lou, *Adv. Mater.* 27 (2015) 4097–4101.
- [32] Y. Lee, D. Thirumalai, C. Hyeon, *J. Am. Chem. Soc.* 139 (2017) 12334–12337.
- [33] Q.H. Wei, Q.X. Ma, P.P. Zuo, H.L. Fan, S.J. Qu, W.Z. Shen, *ChemCatChem* 10 (2018) 1019–1026.
- [34] H. Lin, Z. Hao, X.R. Zheng, Y.M. Huang, P. Zhang, Q.W. Chen, *Sci. Rep.* 2 (2012) 986–994.
- [35] V. Stevanović, M. D’Avezac, A. Zunger, *J. Am. Chem. Soc.* 133 (2011) 11649–11654.
- [36] J. Ajay, K.R. Patil, C.V. Rode, *ChemPlusChem* 78 (2013) 1384–1392.
- [37] Z.M. Huang, W. Zhou, C. Ouyang, J. Wu, F. Zhang, J.G. Huang, Y.Q. Gao, J.H. Chu, *Sci. Rep.* 5 (2015) 10899–10907.
- [38] Y.R. Liu, B.C. Zhang, J.K. Feng, S.L. Xiong, *RSC Adv.* 5 (2015) 26863–26871.
- [39] H.Y. Chen, A. Sayari, A. Adnot, F. Larachi, *Appl. Catal. B Environ.* 32 (2001) 195–204.
- [40] D.X. Yan, J.Y. Xin, C.Y. Shi, X.M. Lu, L.L. Ni, G.Y. Wang, S.J. Zhang, *Chem. Eng. J.* 323 (2017) 473–482.
- [41] L.F. Liao, Y. Liu, Z.Y. Li, J.P. Zhuang, Y.B. Zhou, S.Z. Chen, *RSC Adv.* 6 (2016) 94976–94988.
- [42] K.W. Omari, J.E. Besaw, F.M. Kerton, *Green Chem.* 14 (2012) 1480–1487.
- [43] H. Choudhary, S. Nishimura, K. Ebitani, *Appl. Catal. A Gen.* 458 (2013) 55–62.
- [44] W. Huang, S.J. Ding, Y. Chen, W.J. Hao, X.Y. Lai, J. Peng, J.C. Tu, Y. Cao, X.T. Li, *Sci. Rep.* 7 (2017) 5220–5231.
- [45] X.H. Zhou, W.M. Kang, W. Xu, B.W. Cheng, *RSC Adv.* 5 (2015) 84535–84542.
- [46] E. Hayashi, T. Komanoya, K. Kamata, M. Hara, *ChemSusChem* 10 (2016) 654–658.
- [47] Z.Y. Gui, S. Saravanamurugan, W.R. Cao, L. Schill, L.F. Chen, Z.W. Qi, A. Riisager, *ChemistrySelect* 2 (2017) 6632–6639.
- [48] Y.W. Cheng, X. Li, L.J. Wang, Q.B. Wang, *Ind. Eng. Chem. Res.* 45 (2006) 4156–4162.
- [49] S.A. Chavan, S.B. Halligudi, D. Srinivas, P. Ratnasamy, *J. Mol. Catal. A Chem.* 161 (2000) 49–64.
- [50] S. Todorova, H. Kolev, J.P. Holgado, G. Kadinov, Ch. Bonev, R. Pereguez, A. Caballero, *Appl. Catal. B Environ.* 94 (2010) 46–54.
- [51] H. Chen, M. Yang, S. Tao, G. Chen, *Appl. Catal. B Environ.* 209 (2017) 648–656.
- [52] A.C. Zhang, W.W. Zheng, J. Song, S. Hu, Z.C. Liu, J. Xiang, *Chem. Eng. J.* 236 (2014) 29–38.
- [53] J.H. Zhang, Y.B. Li, L. Wang, C.B. Zhang, H. He, *Catal. Sci. Technol.* 5 (2015) 2305–2313.